# Characterization of novel KCNH2 mutations in type 2 long QT syndrome manifesting as seizures.

Dagmar Keller, Julie Grenier, Georges Christé, Frédérique Dubouloz, Stephan Osswald, Marijke Brink, Eckhard Ficker, Mohamed Chahine

# Characterization of novel KCNH2 mutations in the long QT syndrome type 2 manifesting as seizures

Dagmar I. Keller[1,2], Julie Grenier[3], Georges Christé[4], Frédérique Dubouloz[2], Stefan Osswald[1], Marijke Brink[2], Eckhard Ficker[5], Mohamed Chahine[3]

Running title: Characterizing novel KCNH2 mutations

Conflicts of Interest: None

[1]Cardiology Department and [2]Cardiobiology Research Laboratories, University Hospital Basel, Switzerland

[3]Le centre de recherche Université Laval Robert-Giffard, Quebec, Canada

[4]INSERM, Lyon, France

[5]Case Western Reservation University, Cleveland, USA

Correspondence to:

Mohamed Chahine, Ph.D

Le Centre de recherche Université Laval Robert-Giffard

2601 chemin de la Canardière

Québec (Québec) G1J 2G3 Canada

Tél: (418) 663-5747 #4723

Fax: (418) 663-8756

E-mail: mohamed.chahine@phc.ulaval.ca

## Summary:

LQTS type 2 is caused by mutations in the *KCNH2* gene leading to a reduction of $I_{Kr}$ current and loss of hERG channel function. We identified three novel *KCNH2* mutations, Y493F, A429P and del234-241, in the index patients with mostly typical ECG features of LQTS2 and auditory induced syncope interpreted as "seizure" and Sudden Cardiac Death. The biochemical data revealed a trafficking defect while the biophysical data revealed a loss of function when mutated hERG channels were co-expressed with the WT.

We concluded that "seizure" must be likely due to cardiac syncope as a consequence of mutation-induced loss of function of the IKr current.

## Structured Abstract:

**Background:** The Long QT Syndrome (LQTS) is characterized by QTc-prolongation leading to Torsades de Pointes and Sudden Cardiac Death. LQTS type 2 (LQTS2) is caused by mutations in the *KCNH2* gene leading to a reduction of $I_{Kr}$ current and loss of hERG channel function by different mechanisms. Triggers for life-threatening arrhythmias in LQTS2 are often auditory stimuli.

**Objectives:** The aim of this study was to screen *KCNH2* for mutations in patients with LQTS2 on the ECG and auditory induced syncope interpreted as "seizure" and Sudden Cardiac Death, and to analyse their impact on the channel function in vitro.

**Methods:** The *KCNH2* gene was screened for mutations in the index patients of three families. The novel mutations were reproduced *in vitro* using the site directed mutagenesis and characterized using the Xenopus expression system in voltage clamp mode.

**Results:** We identified novel *KCNH2* mutations, Y493F, A429P and del234-241, in the index patients with mostly typical ECG features of LQTS2. The biochemical data revealed a trafficking defect while the biophysical data revealed a loss of function when mutated hERG channels were co-expressed with the WT.

**Conclusions:** In all families at least one patient carrying the mutation had a history of "seizure" after auditory stimuli, which is a major trigger for arrhythmic events in LQTS2. In conclusion "seizure" must be likely due to cardiac syncope as a consequence of mutation-induced loss of function of the IKr current.

**Keywords:** Long QT Syndrome type 2; sudden cardiac death; seizure; *KCNH2*; potassium loss of $I_{Kr}$ channel function

## 1. Introduction

The Long QT Syndrome (LQTS) is an inherited electrical cardiac disorder characterized by prolongation of the ventricular repolarization leading to syncope and Sudden Cardiac Death (SCD) by Torsades des Pointes (TdP) degenerating into ventricular fibrillation. To date, ten LQTS phenotypes are known that are caused by mutations in the cardiac ion channels and their linker proteins (http://www.fsm.it/cardmoc/). The second most frequent LQTS phenotype is the LQTS type 2 (LQTS2), accounting for 35-40% of the LQTS phenotypes and mutations. LQTS2 is caused by mutations in the *KCNH2* gene, encoding the alpha subunit of the hERG potassium channel underlying the $I_{Kr}$ current. Functional studies of *KCNH2* mutations in *in vitro* models usually demonstrate a reduction of $I_{Kr}$ currents by different biophysical mechanisms most often due to trafficking defects (1). A dominant negative effect results from current reduction of the tetrameric channel complex.

Diagnosis of LQTS2 is made on the 12-lead surface ECG showing a prolonged QTc interval with low T-wave amplitude and a double notched T-wave morphology (2,3). Specific triggers can precipitate arrhythmic events in patients with the LQTS, which are auditory stimuli and noise in the LQTS2 (3). TdP can lead to syncope but could degenerate into ventricular fibrillation leading to SCD.

The aim of this study was to phenotype and genotype three families with previous history of seizure and SCD with typical LQTS2 on the 12-lead surface ECG. Mutations analysis of *KCNH2* revealed three novel mutations: Y493F, A429P and del234-241. *In vitro* expression of the mutations showed a loss of hERG potassium channel function by reduction of the current, suggesting a dominant-negative effect. The common clinical feature in the families was the occurrence of seizure triggered by noise (alarm clock or telephone ringing). Biochemical and biophysical mechanisms leading to the decrease in $I_{Kr}$ are discussed

## 2. Methods

### *2.1. Clinical evaluation and molecular genetics*

Written informed consent was obtained from participating members of families 1-3 in accordance to the study protocol approved by the local ethics committee of the University Hospital of Basel, Switzerland. The investigation conforms to the principles outlined in the Declaration of Helsinki. Participating members underwent detailed clinical examinations including consecutive 12-lead surface ECG's.

Genomic DNA was extracted from peripheral lymphocytes. In the index patients of families 1-3, all coding exons of *KCNH2* were amplified by polymerase chain reaction (PCR) using primers designed in intronic flanking sequences. Denaturating high performance liquid chromatography (DHPLC) was performed on DNA-amplification products on at least one temperature condition. Abnormal DHPLC profiles were analysed by sequence reaction in both strands of the exon, using a big dye termination mix and analysed by cycle sequencing using an automated laser fluorescent DNA sequencer (ABI Prism 377, Applied Biosystems, Foster City, CA, USA). After identification, the specific mutations were directly searched in the family members by PCR and sequenced in both strands as described above. Mutations were absent in chromosomes from 200 normal subjects.

### *2.2. Mutagenesis*

hERG mutations were generated using site-directed mutagenesis and were performed on the hERG-pGH19 (6.9kb) construct provided by Dr. Gail A. Robertson (University of Wisconsin-Madison Medical School, USA). The following mutagenetic sense and anti-sense primers were used.

For hERG/del 234-241:

5'-GCACGCAGCGCCGCGC↓ AGATCGCGCAGGCACTG-3' and

5'-CAGTGCCTGCGCGATCT↑ GCGCGGCGCTGCGTGC-3'

For hERG/A429P:

5’-CTTCACACCCTACTCG**CCT**GCCTTCCTGCTGAAGG-3’

5’-CCTTCAGCAGGAAGGCAG**G**CGAGTAGGGTGTGAAG-3’

For hERG/Y493F:

5’-CGCATCGCCGTCCAC**TTC**TTCAAGGGCTGGTTC-3’

5’-GAACCAGCCCTTGAA**GAA**GTGGACGGCGATGCG-3’

Mutagenesis was conducted according to the Quick Change™ kit from Stratagene (La Jolla, CA) and the mutated sites were confirmed by automatic sequencing. Capped mRNAs of hERG wild type (WT) and mutated were produced using the SP6 mMESSAGE mMACHINE™ from Ambion (Austin, TX, USA).

### *2.3. Oocyte preparation and expression of hERG potassium channels*

The preparation of *Xenopus* oocytes was previously described.(4) Briefly, oocytes were subjected to collagenase treatment 2 mg/ml during 2.5-3 hours, stage V or VI oocytes were microinjected with 5 ng capped mRNA encoding either WT, mutant hERG or both. The oocytes were maintained at 18ºC in a 2-fold diluted solution of Leibovitz's L-15 medium (Gibco, Grand Island, N.Y., USA) enriched with 15 mM 4-(2-hydroxyethyl)-1-piperazine-methanesulfonic acid (HEPES, pH 7.6, adjusted with NaOH), 1 mM glutamine, and 50 µg/µl gentamycin. Oocytes were used for experiments 1-3 days after injection. The macroscopic potassium currents from the mRNA-microinjected oocytes were recorded using voltage-clamp technique with two 3M KCl-filled microelectrodes. Membrane potential was controlled by a Warner oocyte clamp (Warner Instrument Corp., Hamden, CT). Voltage commands were generated by computer using pCLAMP software version 7 (Axon Instruments, Inc., Foster City, CA). Currents were filtered at 2 kHz (-3 dB; 4 pole Bessel filter).

### *2.4. Solutions*

The Ringer's bathing solution contained (mM): 116 NaCl, 2 KCl, 1.8 $CaCl_2$, 1.0 $MgCl_2$, 5 HEPES; pH was adjusted to 7.6 at 22ºC with NaOH. All experiments were carried out at room temperature (22ºC).

### *2.5. Analysis of electrophysiological data*

A standard two-pulse protocol was applied from a holding potential at –80 mV. A 2 seconds duration prepulse (P1) to various potentials ($V_{P1}$) from –80 to +60 mV in 10 mV increments was followed by a 2 sec test pulse (P2) to –60 mV ($V_{P2}$). The current magnitude at the end of the first pulse ($I_{P1}$) and the peak current amplitude short after the beginning of the second pulse ($I_{P2}$) were measured.

*Accounting for the voltage dependence of the endogenous current:*

The endogenous current was recorded in non-injected oocytes (e.g.: Figure 4A lower panel). The endogenous current ($I_{ENDO1}$) was measured at end of prepulse P1 and at time of peak hERG current in the test pulse P2 ($I_{ENDO2}$). Both measurements were well accounted for by exponential functions of voltage VP1 in prepulse P1:

$$I_{ENDO1} = g_{ENDO} * \exp(V_{P1}/k_{1V}) \quad (1)$$

$$I_{ENDO2} = g_{ENDO} * fr * \exp(V_{P1}/k_{2V}) \quad (2)$$

with fr being a factor between 0 and -1 reflecting the remaining endogenous current during pulse P2 after being activated during pulse P1 and taking into account the fact that the reversal voltage of the endogenous current is positive to the voltage in pulse P2 i.e. –60 mV. Figure 5A shows the fitting functions (3) and (7) adjusted to the averaged endogenous current data sets yielding values: $g_{ENDO}$=3.44 nA; fr=-0.288; $k_{1V}$=26.8 mV; $k_{2V}$=23.6 mV. Functions were included in the next procedure to account for the endogenous current that could corrupt data analysis of the hERG current.

*Global fitting analysis of features of the hERG current:*

The voltage-dependence of total oocyte currents $I_{P1}$ and $I_{P2}$ may respectively be described by the expressions:

$$y1 = I_{ENDO1}(V_{P1}) + g_{hERG}*(V_{P1}-E_{rev}) * h_{inf}(V_{P1}) * r(V_{P1}) \quad (3)$$

and

$$y2 = I_{ENDO2}(V_{P1}) + g_{hERG}*(V_{P2}-E_{rev}) * h_{inf}(V_{P1}) \quad (4)$$

where:

$$g_{hERG}*(V_{P1}-E_{rev}) \quad (5)$$

expresses the voltage dependence of the fully activated and non-inactivated hERG current. This expresses the ohmic behaviour of the open hERG channel (5).

$h_{inf}(V_{P1})$ is the voltage-dependent value of the activation variable at the end of pulse P1:

$$h_{inf}(V_{P1}) = 1/(1+\exp((V_{P1}-V_{ha})/k_a)) \quad (6)$$

with $V_{ha}$ being the half activation potential and $k_a$ the slope factor;

$r(V_{P1})$ is the voltage dependent rectification function:

$$r(V_{P1}) = 1/(1+\exp((V_{P1}-V_{hr})/k_r)) \quad (7)$$

with $V_{hr}$ being the half rectification potential and $k_r$ the slope factor;

$I_{ENDO1}$ and $I_{ENDO2}$ are the endogenous oocyte currents that respectively correspond to functions (1) and (2) where $k_{V1}$ and $k_{V2}$ were both set at a value of 25 mV.

A global fitting procedure simultaneously adjusted functions y1 and y2 by a least-squares algorithm (Simplex) to the experimental series of data couples: $I_{P1}$ versus$V_{P1}$ and $I_{P2}$ versus $V_{P1}$ of each cell. The reversal voltage of the hERG current $E_{rev}$ was fixed at -77 mV, parameters $g_{ENDO}$, fr, $g_{hERG}$, $V_{ha}$, $k_a$, $V_{hr}$ and $k_r$ were adjusted for the best simultaneous fit of both data sets. The values of $g_{hERG}$, $V_{ha}$, $k_a$, $V_{hr}$ and $k_r$ are reported in Table 1.

An example of the fitting is given in Figure 5B showing the adequacy of the functions to represent the data sets.

This analysis is consistent with the theoretical description of Sanguinetti et al (6).

### *2.6. Western blot analysis*

Antibodies used in the present study have been described previously (7). Briefly, The anti-hERG polyclonal antibody used in Western blots was generated in rabbits against a glutathione-*S*-transferase (GST) fusion protein containing the last 112 amino acids of hERG (residues 1048-1159). hERG antiserum was either purified on an affinity column consisting of a short COOH-terminal peptide corresponding to hERG residues 1102-1121 (TLTLDSLSQVSQFMACEELP) or the entire fusion protein. Briefly, HEK/hERG cells were solubilized for 1h at 4°C in lysis buffer containing 150mM NaCl, 1mM EDTA, 50mM Tris, pH 8.8, 1% Triton X-100 and protease inhibitors (Complete, Roche Diagnostics, Indianapolis, IN, USA). Proteins were separated on SDS polyacrylamid gels, transferred to polyvinylidene difluoride membranes and developed using hERGbasic antibody followed by ECL plus (GE Healthcare, Piscataway, NJ, USA).

### *2.7. Statistical analysis*

A Student's t-test on two independent samples was performed to compare parameters of each of the mutated hERG currents to those of the WT. In figures, the significance of differences was labelled * for $p<0.05$, ** for $p<0.01$ and *** for $p<0.01$.

## 3. Results

### *3.1. Identification of three novel KCNH2 mutations and family screening*

We identified three novel *KCNH2* mutations in the index patients of the families (patient II-1 of family 1, patient II-1 of family 2, patient II-2 of family 3). In patient II-1 of family 1 (Figure 1A), a heterozygous change of Tyrosin (TAC) to Phenylalanin (TTC) resulted in the missense mutation Y493F (Figure 1B). Y493F is localized at the end of the S2-S3 linker region of the hERG potassium channel. In patient II-1 of family 2 (Figure 2A), a heterozygous change of Alanin (GCT) to Prolin (CCT) resulted in the A429P mutation (Figure 2B). A429P is localized at the beginning of S1-S2 of the hERG potassium channel. A deletion in exon 2, del234-341 TGCCGCGC in codon 78 was identified in patient II-2 of family 3 (Figure 3A, B). This mutation at the beginning of the N-terminal introduces a stop codon 62 amino acids further the 78 codon. During family screening Y493F was identified in individual III-1 of family 1, A429P in individuals III-1 and IV-2 and del234-341 was identified in individuals II-1 and III-3 in family 3.

### *3.2. Phenotypes of the families*

#### *3.2.1. Family 1*

The index patient II-1 (male, born 1951) was diagnosed with seizure in childhood. Seizure always occurred in the morning after auditory stimuli. Diagnosis of LQTS2 was made after presyncope at the age of 54 yrs. The 12-lead ECG showed typical LQTS2 with QTc 525 ms (Figure 1C). Family history revealed that his father (I-1) died of rhythm problems at the age of 52 yrs. The daughter (III-2) died of SCD at the age of 14 yrs; she was diagnosed with seizure in early childhood. The son of the index patient (III-1), born 1981, was diagnosed with seizure at the age of 9 yrs. He was treated with carbamazepin. After the age of 18 yrs he had no symptoms of seizure anymore, still taking carbamazepin. Diagnosis of LQTS2 was made during family screening with QTc 539 ms and typical T-wave morphology (data not shown). Patients II-1 and III-1 both showed LQTS2 on the ECG and carried the Y493F *KCNH2*

mutation; both received an Implantable Cardioverter Defibrillator (ICD). No ICD discharges were documented in both patients until present.

Data from electroencephalograms (EEG) are available for patient III-1. Under therapy with carbamazepine, the EEG before ICD implantation showed normal baseline activity with minor functional disturbance bitemporo-occipital.

### *3.2.2. Family 2*

The index patient II-1 (female, born 1930) was diagnosed with LQTS2 at the age of 75 yrs having TdP during anaesthesia to fix her broken arm. She was diagnosed with auditory reflex epilepsy in childhood with syncope's always after telephone ringing. No EEG data were available at this time. Since childhood she was treated with phenytoin and had about ten syncopes until the age of 40 yrs. From age 40 to 75 she had no symptoms at all still taking phenytoin. Above described TdP occurred under phenytoin medication. Her present 12-lead ECG showed typical LQTS2 with QTc 462ms (Figure 2C). During family screening her only daughter III-1, born 1970, was diagnosed with LQTS2 with QTc 476 ms (data not shown). In contrast she had no symptoms. Her daughter (IV-2), born 1999, had one syncope while standing. Patients II-1, III-1 and IV-2 carry the A429P *KCNH2* mutation; they all are being treated with beta-blocker.

### *3.2.3. Family 3*

In family 3, patient I-2 (female) died at the age of 43 yrs after telephone ringing. The index patient II-2 (male, born 1966) suffered from syncope during sports in childhood. His 12-lead ECG showed QTc 467 ms with a broad T-wave, not typical for LQTS2 (Figure 3C). In contrast his brother II-1 (born 1965) suffered from seizure in childhood and showed typical LQTS2 on the 12-lead ECG with QTc 464 ms (Figure 3C). During family screening the daughter (III-3, born 1992) of the index patient was diagnosed with LQTS2 on the ECG,

having a history of dizziness. In patients II-2, II-1 and III-3 the *KCNH2* mutation del234-341 was found. Patients II-2 and II-1 received an ICD, while patient III-3 is being treated with beta-blocker. No EEG data are available for this family.

### *3.3. Macroscopic recordings of hERG currents*

As shown in Figure 4A, the expression of mutation hERG/Y493F yielded a considerably lower current than the WT. When the mutant hERG was co-expressed with the WT, the current amplitude was reduced to about half of that in the WT. The two other mutations, A429P and del234-241, when expressed alone, failed to express more than the endogenous current observed in non-injected oocytes (Figure 4B and C, middle panels). When co-expressed with WT hERG (Figure 4B and C, lower panels), each of them developed currents that were roughly half smaller than when the WT was expressed alone.

In order to accurately evaluate the macroscopic properties of these currents, a global fitting procedure was used to evaluate steady-state activation versus voltage relation and apparent steady-state rectification versus voltage relation by simultaneously fitting theoretical functions to current versus voltage data sets as measured at the end of pulse P1 and at peak current at the beginning of pulse P2 (see methods). A function accounting for endogenous current, that had been derived from analysis of the endogenous current in non-injected oocytes, served to automatically prevent distortions of the hERG currents (see methods).

After applying this procedure to data sets from each of the cells, the endogenous current was subtracted and average hERG current/voltage relations were plotted in for currents $I_{P1}$ and $I_{P2}$ Figure 5C, D, E and F. This allows direct comparison of the voltage dependent features between mutated hERG co-expressed with the WT and the WT hERG expressed alone. The average values of the individual parameters resulting from the global fitting analysis are reported for each expression case in Table 1.

Co-expression of mutation del234-241 with the WT resulted in a two-fold reduction in the current at the end of pulse P1 (Figure 5C), in agreement with the half lower maximal hERG conductance (Table 1). This is in line with the absence of changes in activation (Figure 5D and Table 1) and rectification parameters (Table 1). When mutation A429P was co-expressed with the WT, the current during pulse P1 was only decreased by 22% from that of the WT (Figure 5C) whereas the maximal hERG conductance was reduced two-fold (Table 1). This is the result of the combination of a negative shift in the voltage for half activation $V_{ha}$ (Figure 5D and Table 1) and a positive shift in the voltage for half rectification $V_{hr}$ (Table 1). Both of these changes, although not statistically significant, caused a larger availability of the current, while their respective slope factors $k_a$ and $k_r$ did not differ from those of the WT (Table1). Of the three mutations studied here, only mutation Y493F yielded current when expressed alone. Although the maximal apparent current at the end of pulse P1 was only 40% less than in the WT (figure 5E), the maximal conductance was 6 times lower than that of the WT (Table 1). This discrepancy resulted from a shift of the activation curve by 12 mV in the hyperpolarizing direction (Figure 5F and Table 1). There was a slight but significant increase (1.85 mV) in the value of the negative slope factor $k_a$ whereas, for the apparent rectification versus voltage, only the slope factor $k_r$ was affected, i.e. increased by 3.3 mV (Table 1). When mutation Y493F was co-expressed with the WT, the maximal macroscopic current $I_{P1}$ was only 27% less than that of the WT alone (Figure 5E) whereas the maximal hERG conductance was lowered by half as compared to the WT alone (Table 1). This may be related to a shift by 6 mV in the depolarising direction of the half rectification voltage $V_{hr}$, which, although not statistically significant, caused an increase in the availability of the current (Figure 5E), while the slope factor $k_r$ of the rectification curve did not change (Table 1). The voltage for half activation $V_{ha}$ was not significantly affected whereas the absolute value of the slope factor $k_a$ was increased by 1.2 mV (Table 1).

### *3.4. Western blot analysis of hERG mutations*

Figure 6 shows Western blots of the hERG mutations compared to the wild type. The hERG antibody used is described in the methods. As can be seen, hERG Y493F produces a small amount of fully-glycosylated (fg) cell surface hERG (160 kDa). This is possibly a hypomorphic mutation that may be rescued by low incubation temperature or a hERG blocker such as astemizole. However, hERG A429P can only be detected as a core-glycosylated (cg), endoplasmic reticulum (ER) retained protein of about 135 kDa at 37$^{o}$C.

Interestingly the hERG deletion (del 234-241) produces quite surprisingly fully-glycosylated protein as can be seen from the blot. Evidently, the amount of protein is severely reduced when compared to WT or even to the other missense mutations shown on this blot.

## 4. Discussion

We report three novel *KCNH2* mutations in three families with the LQTS2 and a previous history of seizure with loud noise as the common trigger. *In vitro* expression of the mutations Y493F, A429P and del234-241 *KCNH2* showed a loss of hERG potassium channel function by reduction of the current, suggesting a trafficking defect.

### *Genotype-phenotype correlation and triggers for arrhythmia*

Except for patient II-2 of family 3, all affected family members showed typical LQTS2 ECG phenotypes, consistent with the positive *KCNH2* genotype. The ECG of patient II-2 of family 3 shows a broad T-wave with a delayed onset of the upstroke part of the T-wave without double notch and low amplitude, more consistent with a LQTS type 1 or 3 ECG (Figure 3C).(2) No mutations could be identified in the responsible genes *KCNQ1* (LQTS1) and *SCN5A* (LQTS3) in this patient (data not shown). An important observation in the LQTS is the change of the ECG phenotype appearance by recording serial ECG. Still in our patient

repetitive ECG never showed the typical LQTS2 phenotype. This might be due to additional genetic and other factors influencing the phenotype caused by the major gene mutation.

In at least one member of all families, seizure was diagnosed in childhood. Unfortunately no EEG data are recorded from this time. Seizure always occurred after telephone or alarm clock ringing usually in the morning. This is consistent with the known triggers for arrhythmias in the LQTS2 (3).

Mutations in the Y493 residue of *KCNH2* have previously been found. The first mutation was Y493X in a family with the LQTS.(8) Lupoglazoff described a heterozygous Y493C mutation in a patient with fetal bradycardia (9). Functional studies are not available for these mutations.

The interpretation of seizure in these families is likely due to cardiac syncope as a consequence of malignant ventricular arrhythmias. EEG data of only one patient are available showing minor functional disturbance bitemporo-occipital. In this patient the question arises whether the underlying primary cause of seizure might be due to a channel mutation in the brain. In a recent paper of Gurnett et al. (10) susceptibility gene for human epilepsy include genes coding for neuronal sodium channels (*SCN1A, SCN1B, SCN2A*), calcium channels (*CACNA1A, CACNA1H, CACNB4*), potassium channels (*KCNQ2, KCNQ3, KCNA1*), genes for acetylcholine and GABA receptor and other genes. Mutations in *KCNQ2* and *KCNQ3* alter the structure of the pore region and/or COOH-terminal cytoplasmic domain (for review, see (11)). These alterations lead to a potential loss or gain of function, or dominant negative effects. The hERG gene is expressed in the heart where it is responsible for the $I_{Kr}$ current, but transcript variants encoding distinct isoforms have been identified in the brain and skeletal muscle tissues (12,13). The properties of hERG channels match with the gating properties of Eag-related potassium channels (14). The hERG gene shares similarity in the sequence with the Dosophila ether-a-go-go (eag) gene. The mutant phenotype of the eag-gene was initially attributed to an increase in neuronal excitability and transmitter release at the neuromuscular

junction (15). This observation may explain a possible link between seizure and cardiac arrhythmias

***Pathophysiological implications of mutated hERG macroscopic current properties***

Evaluation of the pathophysiological consequences is based on the changes in properties of macroscopic currents developed when each mutation is co-expressed with the WT hERG, a situation that mimics the heterozygous condition seen for the present mutations (see §3.1. in Results section).

None of the two mutated hERG del234-241 and A429P gave any current when expressed alone in oocytes (Figure 4). Although hERG del234-241 generates no currents some readout can be seen on the western with this deletion mutant, this was consistent in our four carried out westerns, more experiments are required to clarify this issue. As compared with WT injected oocytes, the half lower whole-cell maximal conductance derived for oocytes injected with either WT + del234-241 or WT + A429P (Table 1) was not accompanied with significant changes in activation and rectification properties.

It should be noted that, at the most negative voltages, activation is incomplete at the end of the first pulse of the two-pulse protocol. Whether this would cause a misevaluation of the characteristics of the activation versus voltage relationship was tested in a computer model of hERG current in which a function of the time constant of activation versus voltage was set to reproduce the properties of the WT hERG current (data not shown).

While part of the lower conductance may be due to non-conducting or non- trafficking of the homotetramers formed with the mutated proteins alone, this part should not exceed $1/16^{th}$ of the maximal current if all other tetramers would traffic and conduct as the WT tetramer. As was previously reported for a number of hERG mutations the lower conductance may be due to negative dominant effect of the mutated form of hERG on the WT (6,16). Such a decrease in hERG conductance may suffice to account for the propensity of the subjects bearing these

mutations to generate arrhythmias, as was confirmed by model simulations (17,18), due to a delayed repolarization of the ventricular action potential.

Regarding the changes caused by mutation Y493F, the situation is not as simple: a very large decrease in conductance when the mutation is expressed alone in oocytes suggests that, when co-expressed with the WT, a small part of the decrease in whole cell conductance shall be due to homotetramers, again either less conductive or in lower numbers at the membrane, e.g. partially defective trafficking. The whole cell maximal conductance when mutation Y493F was co-expressed with the WT was half smaller than for the WT alone. For this mutation, when co-expressed with the WT only a slight increase in the absolute value of the slope factor of the activation versus voltage curve was noted. Whether the combination of these effects would cause a diminished hERG current response during an action potential ought to be tested within a ventricular cell model.

This was done using a ventricular cell model recently developed (19) (http://dx.doi.org/10.1016/j.pbiomolbio.2007.07.022). None of the kinetic changes related to voltage-dependence of activation and apparent rectification was able to affect the duration of the action potential (see Figure 7A) or the amplitude and time-course of the hERG current (Figure 7B). When the decrease by half of the whole cell hERG conductance was inserted into the model, a 9% lengthening of the action potential duration at 90% repolarisation level was found. This is the likely cause of the observed long QT condition and the resulting predisposition to arrhythmias and associated syncope.

***Influence of antiepileptic drugs on the hERG potassium channel***

In our families two patients were treated with antiepileptic drugs: Patient III-1 of family 1 with carbamazepine, patient II-1 of family 2 with phenytoin. Both phenytoin and carbamazepine have been shown to induce concentration-dependent cardiac arrhythmogenic

potential.(20) For phenytoin the mechanism is sought to be an $I_{Kr}$ blocking potential in vitro.(21) The demonstrated loss of channel function caused by the A429P mutation could be theoretically aggravated by the additionally *in vitro* $I_{Kr}$ blocking potential of phenytoin in the patient carrying the mutation. Surprisingly the patient had no cardiac symptoms or seizure for almost 35 years under phenytoin. On the other hand phenytoin was shown *in vivo* to efficiently treat malignant ventricular arrhythmias associated with myocardial infarction (22), whereas in myocardial infarction the function of the hERG channel is not affected. In addition fosphenytoin, a prodrug of phenoytoin, is known to prolong the QT interval and have a possible risk for TdP (http://www.arizonacert.org/). In our patient the QT interval remained prolonged after stopping phenytoin. Thus it remains unclear why the patient was asymptomatic for many years, but it might be in line with the wide phenotype heterogeneity of the LQTS2 influenced by a complex genotype.

***Conclusion***

We describe in this paper auditory-induced cardiac syncope in three families with the LQTS2 carrying either of the Y493F, A429P and del234-241 hERG mutations. The biochemical data revealed a trafficking defect while the biophysical data revealed a loss of function of hERG channels. The clinical, biochemical and biophysical data together demonstrate the severity of the disease in patients carrying these mutations. Patients with unclear "seizure" following auditory stimuli should be evaluated for malignant arrhythmias in the context of a LQTS.

**Funding**

D.I. Keller was supported by grants from the Swiss Heart Foundation and the "Stiftung für Kardiovaskuläre Forschung" University Hospital Basel, Switzerland. This study was supported by grants from the Heart and Stroke Foundation of Québec (HSFQ), the Canadian

Institutes of Health Research, MT-13181. Dr G. Christé received support from the Fédération des Maladies Orphelines (Paris, France) and from the Centre Jacques Cartier (Lyon, France). Dr M. Chahine is a J.C. Edwards Foundation Senior Investigator.

**Acknowledgements**

We thank Dr V. Fressart, UF Cardiogénétique/Myogénétique, GH Pitié-Salpêtrière, Paris, France, for the verification of the mutations; Dr B. Biedermann, Dr P. Rickenbacher and Dr S. Ruegg, University Hospital Basel and Bruderholz Hospital, Switzerland, for providing clinical data.

**Figure legends**

**Figure 1**

**A:** Pedigree of family 1. The index patient is marked by an arrow. Individuals with black squares/circles carry the mutation and the clinical phenotype with symptoms. Patient III-2 died from sudden death at the age of 14 yrs, no genotype- and ECG data are available (grey filled circle).

**B:** Identification of the Y493F mutation in exon 6 *KCNH2*: a heterozygous change of Tyrosin (TAC) to Phenylalanin (TTC) resulted in the missense mutation Y493F.

**C:** ECG of the index patient II-1 with typical LQTS2 with QTc prolongation 525 ms and low amplitude T-wave with double notch.

**Figure 2**

**A:** Pedigree of family 2. The index patient is marked by an arrow. Individuals with black circles carry the mutation and the clinical phenotype with symptoms. Individual III-1 (grey filled circle) carries the mutation but has no symptoms.

**B:** Identification of the A429P mutation in exon 6 *KCNH2*: a heterozygous change of Alanin (GCT) to Prolin (CCT) resulted in the A429P mutation.

**C:** ECG of the index patient II-1 with typical LQTS2 with QTc prolongation 462 ms and low amplitude T-wave with double notch.

**Figure 3**

**A:** Pedigree of family 3. The index patient is marked by an arrow. Individuals with black squares/circles carry the mutation and the clinical phenotype with symptoms. Individual I-2 died from sudden death at the age of 43 yrs after telephone ringing; no genetic data were available (grey-filled circle).

**B:** Identification of the deletion 234-241 in exon 2 *KCNH2*, del234-341 TGCCGCGC in codon 78.

**C:** ECG's of patients II-2 and II-1. The ECG of II-2 does not show typical LQTS2; the T-wave is broad and a double notch is absent, QTc 467ms. The ECG of II-1 shows typical LQTS2 with QTc prolongation 464 ms and low amplitude T-wave with double notch.

**Figure 4**: Representative examples of recordings of currents in response to a classical two-pulse protocol.

**Figure 5**: **A**: Endogenous current values (filled circles) at end of pulse P1 ($I_{ENDO1}$) and at time of peak hERG current at the beginning of pulse P2 ($I_{ENDO2}$). The solid curves result from the fit by functions (1) and (2) respectively. **B**: example of the global fitting with functions (3) and (4) respectively of data series of current measurements at the end of pulse P1 ($I_{P1}$, squares) and current measurements at peak hERG current during pulse P2 ($I_{P2}$, circles) as a function of voltage ($V_{P1}$) in pulse P1. **C** and **E**: currents measured at the end of pulse P1 were plotted after subtraction of the endogenous current (as evaluated by the global fitting procedure) to show the hERG current and allow visual comparison of the voltage-dependent rectification. **D** and **F**: After subtraction of the endogenous current from peak current values measured at the beginning of pulse P2, currents for each cell were normalized to the maximum value at positive voltages, allowing visual comparison of steady-state activation versus voltage relations.

**Figure 6:** Western blot comparing hERG WT and hERG/Y493F, hERG/A429P and hERG/del234-241 transiently expressed in HEK293 cells using Fugene. HEK293 cells were transfected with 1µg of cDNA. hERG WT is expressed as a fully glycosylated, mature 160-kDa form (fg) and a core-glycosylated, ER resident 135-kDa form (cg). hERG/Y493F expresses considerably less fg hERG protein. For A429P the protein as fg is absent. hERG/del234-241 expresses considerably less hERG protein either as full glycosylated (fg) or core glycosylated (cg) form than WT hERG protein.

**Figure 7**: Model study of the effects of changes in hERG properties as induced by the mutations when co-expressed with the WT on the action potential time course (panel **A**) and on the underlying hERG current of the model cell (panel **B**). When only the changes in activation and rectification due to mutation Y493F are introduced (WT + Y493F no g change, yellow thin line), no change is observed on the shape of the action potential (panel **A**) versus the WT alone (thick black line). When in turn, a two-fold reduction in the whole cell conductance of hERG is included (g/2, thin black line); the action potential duration at 90% repolarisation is lengthened by about 10%.

References

1. Dumaine R, Antzelevitch C. Molecular mechanisms underlying the long QT syndrome. Curr Opin Cardiol 2002;17:36-42.

2. Zhang L, Timothy KW, Vincent GM, Lehmann MH, Fox J, Giuli LCet al. Spectrum of ST-T-wave patterns and repolarization parameters in congenital long-QT syndrome : ECG findings identify genotypes . Circulation 2000;102:2849-2855.

3. Schwartz PJ, Priori SG, Spazzolini C, Moss AJ, Vincent GM, Napolitano Cet al. Genotype-phenotype correlation in the long-QT syndrome : gene-specific triggers for life-threatening arrhythmias . Circulation 2001;103:89-95.

4. Chahine M, Chen LQ, Barchi RL, Kallen RG, Horn R. Lidocaine block of human heart sodium channels expressed in *Xenopus* oocytes. J Mol Cell Cardiol 1992;24:1231-1236.

5. Wang S, Liu S, Morales MJ, Strauss HC, Rasmusson RL. A quantitative analysis of the activation and inactivation kinetics of HERG expressed in Xenopus oocytes. J Physiol 1997;502 ( Pt 1):45-60.

6. Sanguinetti MC, Curran ME, Spector PS, Keating MT. Spectrum of HERG $K^+$-channel dysfunction in an inherited cardiac arrhythmia [published erratum appears in Proc Natl Acad Sci U S A 1996 Aug 6;93(16):8796]. Proc Natl Acad Sci USA 1996;93:2208-2212.

7. Ficker E, Thomas D, Viswanathan PC, Dennis AT, Priori SG, Napolitano Cet al. Novel characteristics of a misprocessed mutant HERG channel linked to hereditary long QT syndrome. Am J Physiol 2000;279:H1748-H1756.

8. Itoh T, Tanaka T, Nagai R, Kamiya T, Sawayama T, Nakayama Tet al. Genomic organization and mutational analysis of *HERG*, a gene responsible for familial long QT syndrome. Hum Genet 1998;102:435-439.

9. Lupoglazoff JM, Denjoy I, Villain E, Fressart V, Simon F, Bozio Aet al. Long QT syndrome in neonates: conduction disorders associated with HERG mutations and sinus bradycardia with KCNQ1 mutations. J Am Coll Cardiol 2004;43:826-830.

10. Gurnett CA, Hedera P. New ideas in epilepsy genetics: novel epilepsy genes, copy number alterations, and gene regulation. Arch Neurol 2007;64:324-328.

11. Lehmann-Horn F, Jurkat-Rott K. Voltage-gated ion channels and hereditary disease. Physiol Rev 1999;79:1317-1372.

12. Wymore RS, Gintant GA, Wymore RT, Dixon JE, McKinnon D, Cohen IS. Tissue and species distribution of mRNA for the $I_{Kr}$-like $K^+$ channel, *erg*. Circ Res 1997;80:261-268.

13. London B, Trudeau MC, Newton KP, Beyer AK, Copeland NG, Gilbert DJet al. Two isoforms of the mouse *ether-a-go-go*-related gene coassemble to form channels with properties similar to the rapidly activating component of the cardiac delayed rectifier $K^+$ current. Circ Res 1997;81:870-878.

14. Trudeau MC, Warmke JW, Ganetzky B, Robertson GA. HERG, a human inward rectifier in the voltage-gated potassium channel family. Science 1995;269:92-95.

15. Ganetzky B, Wu CF. Neurogenetic analysis of potassium currents in Drosophila: synergistic effects on neuromuscular transmission in double mutants. J Neurogenet 1983;1:17-28.

16. Sanguinetti MC, Tristani-Firouzi M. hERG potassium channels and cardiac arrhythmia. Nature 2006;440:463-469.

17. Roden DM, Balser JR. A plethora of mechanisms in the HERG-related long QT syndrome. Genetics meets electrophysiology. Cardiovasc Res 1999;44:242-246.

18. Clancy CE, Rudy Y. Cellular consequences of HERG mutations in the long QT syndrome: precursors to sudden cardiac death. Cardiovasc Res 2001;50:301-313.

19. Pasek M, Simurda J, Orchard CH, Christe G. A model of the guinea-pig ventricular cardiac myocyte incorporating a transverse-axial tubular system. Prog Biophys Mol Biol 2007.

20. Kenneback G, Ericson M, Tomson T, Bergfeldt L. Changes in arrhythmia profile and heart rate variability during abrupt withdrawal of antiepileptic drugs. Implications for sudden death. Seizure 1997;6:369-375.

21. Danielsson BR, Lansdell K, Patmore L, Tomson T. Phenytoin and phenobarbital inhibit human HERG potassium channels. Epilepsy Res 2003;55:147-157.

22. Khan IA, Gowda RM. Novel therapeutics for treatment of long-QT syndrome and torsade de pointes. Int J Cardiol 2004;95:1-6.

**A**

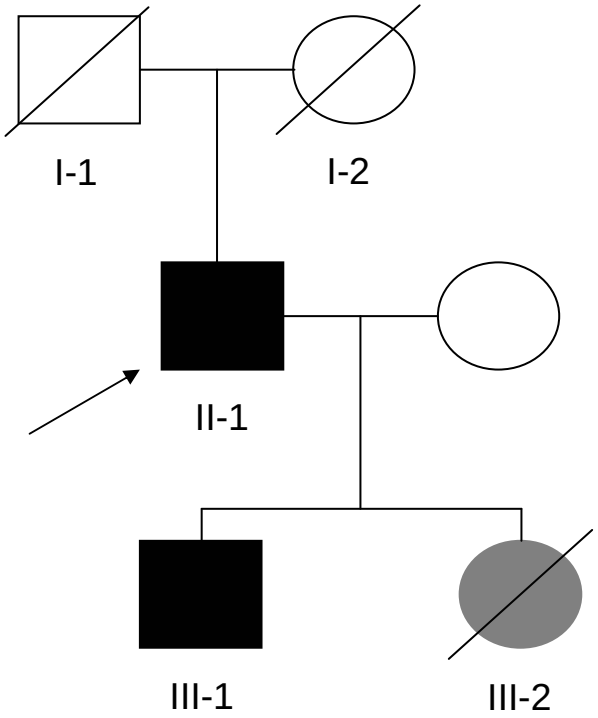


**B**

Y493F *KCNH2*

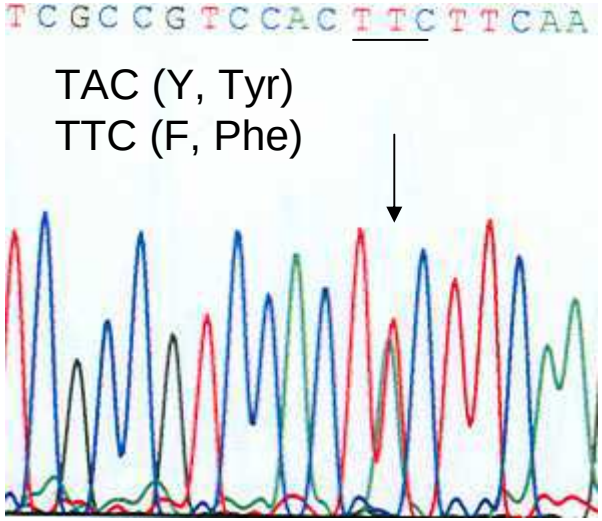


**C**

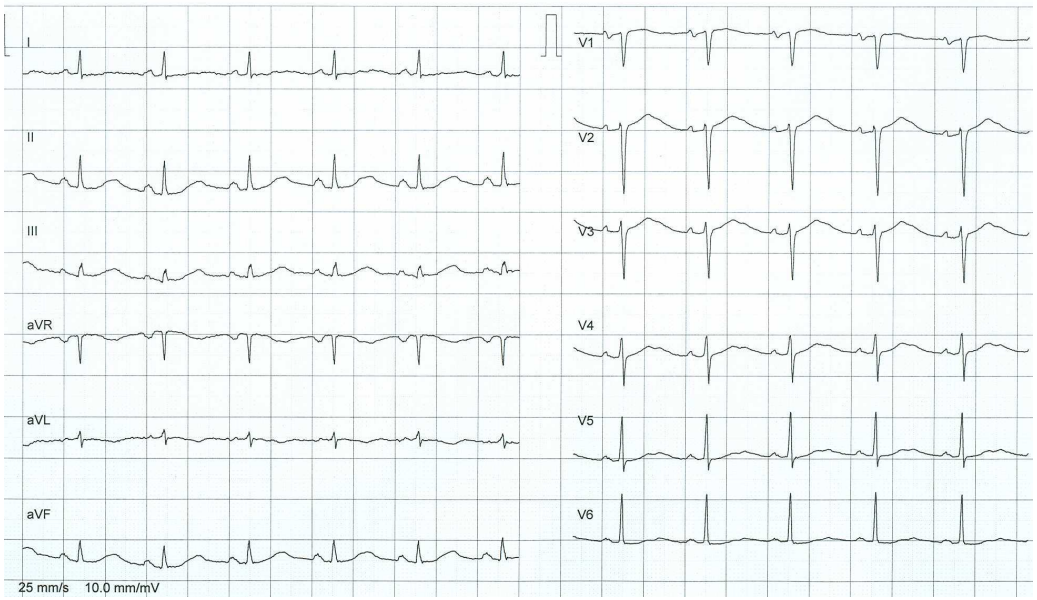


Figure 1

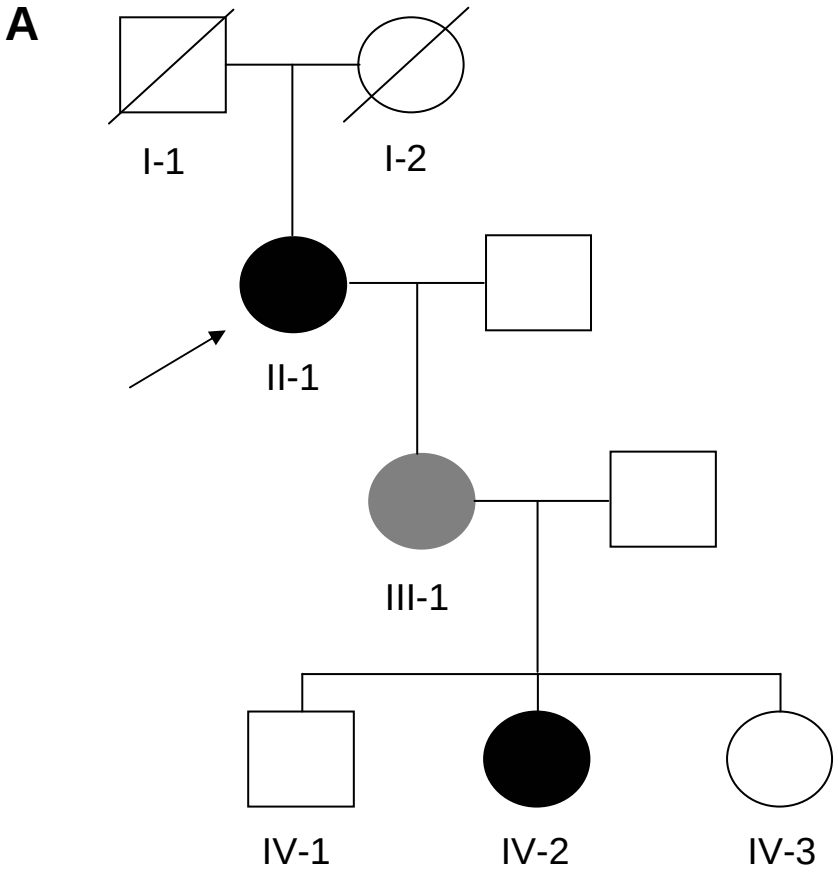
A
I-1
I-2
II-1
III-1
IV-1
IV-2
IV-3

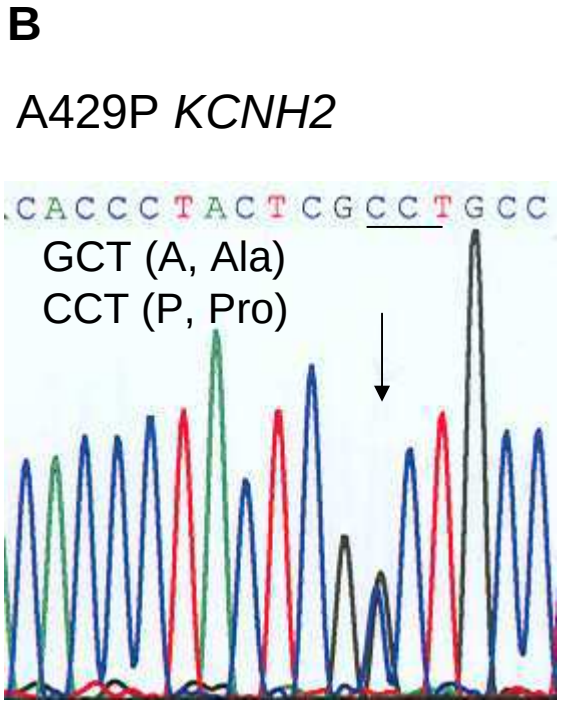
B
A429P *KCNH2*
CACCCTACTCGCCTGCC
GCT (A, Ala)
CCT (P, Pro)

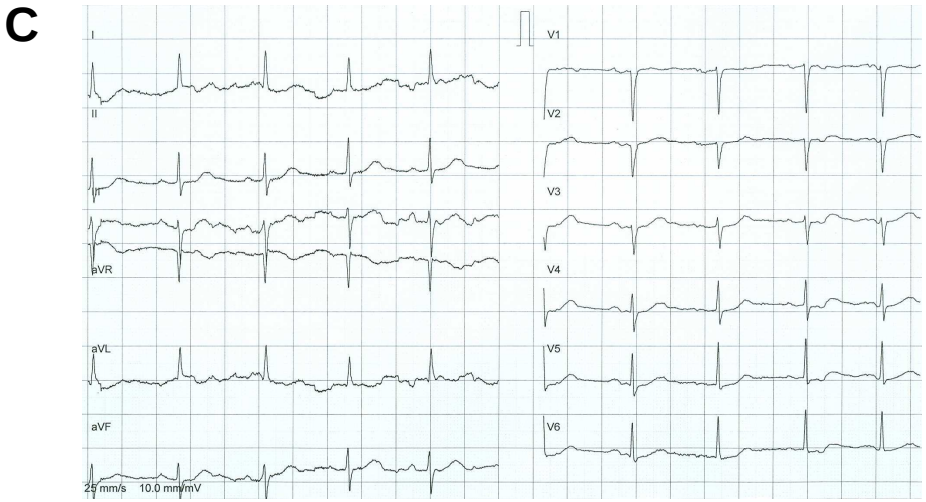
C
I
II
III
aVR
aVL
aVF
V1
V2
V3
V4
V5
V6
25 mm/s 10.0 mm/mV

Figure 2

**A**

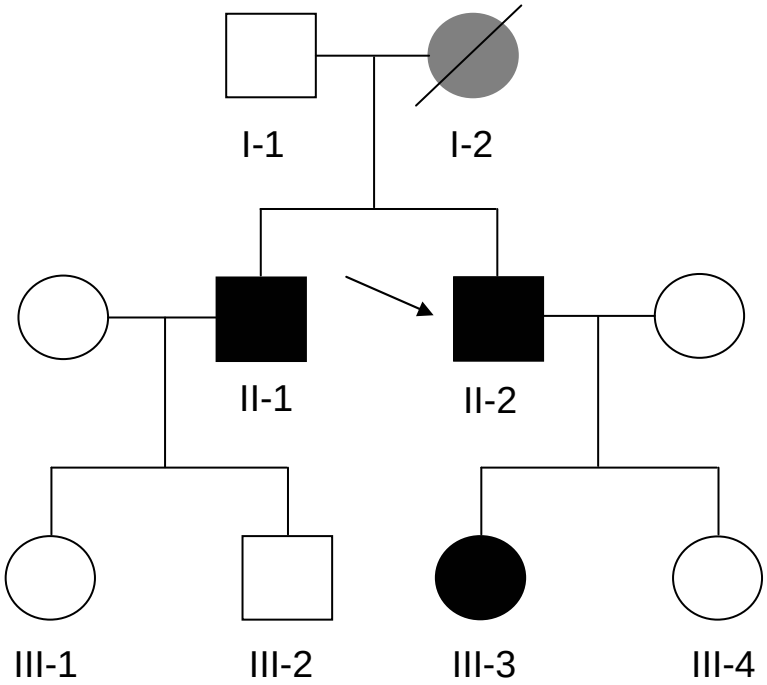


**B**

del234-241 *KCNH2*

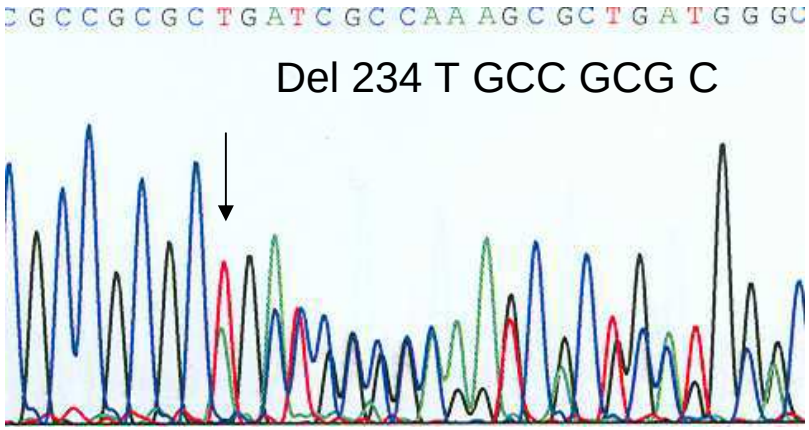


**C** II-2

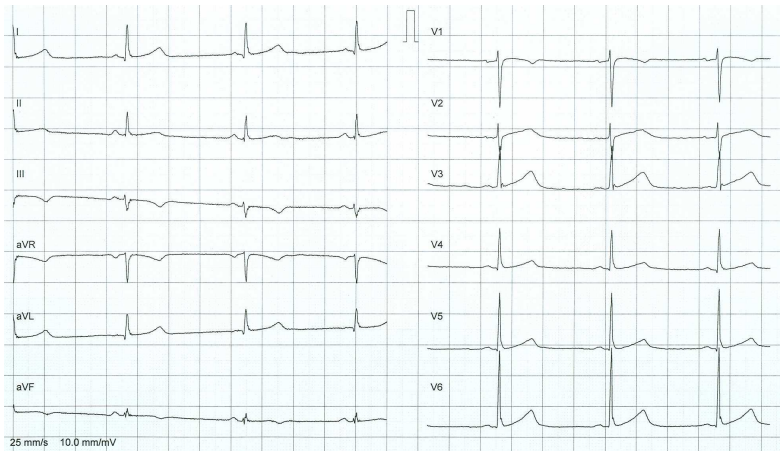


II-1

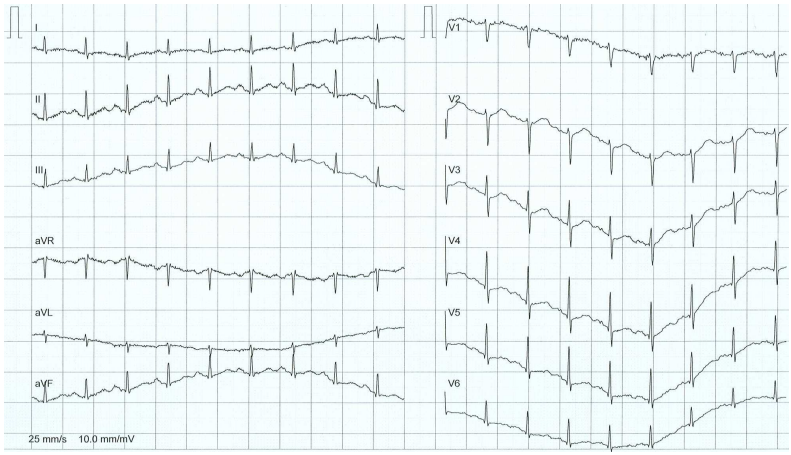


Figure 3

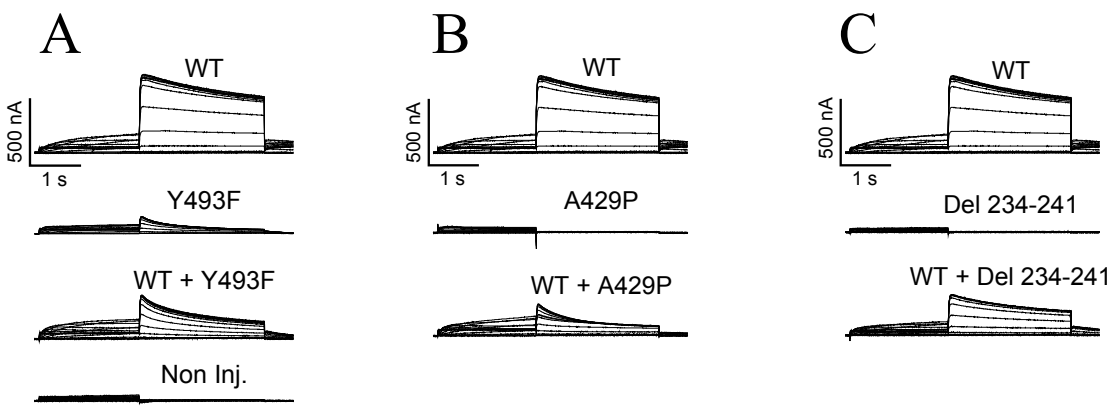
A
WT
500 nA
1 s
Y493F
WT + Y493F
Non Inj.
B
WT
500 nA
1 s
A429P
WT + A429P
C
WT
500 nA
1 s
Del 234-241
WT + Del 234-241

Figure 4

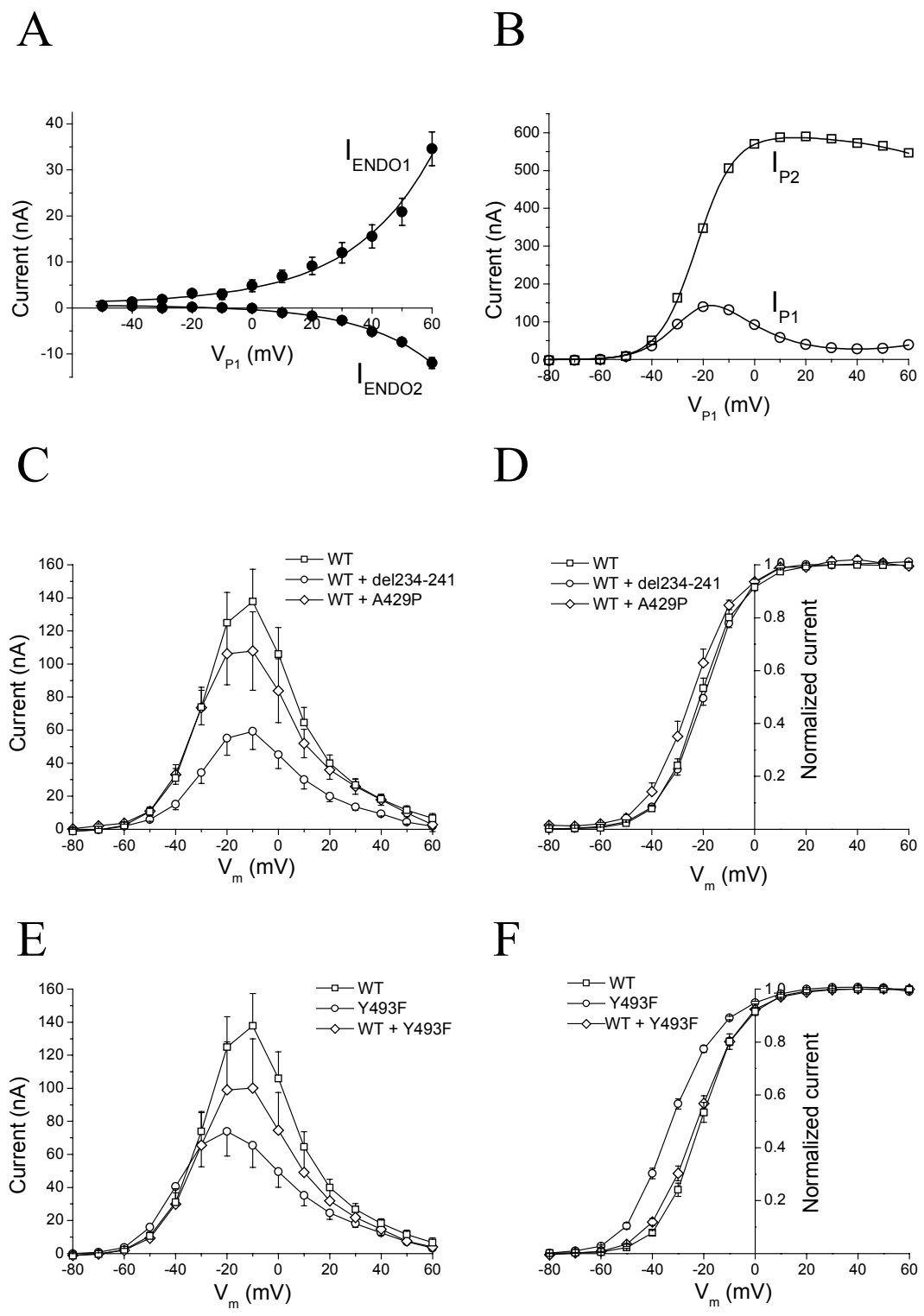
A
B
C
D
E
F
Current (nA)
$I_{ENDO1}$
$I_{ENDO2}$
$V_{P1}$ (mV)
$I_{P2}$
$I_{P1}$
WT
WT + del234-241
WT + A429P
$V_m$ (mV)
Normalized current
Y493F
WT + Y493F

Figure 5

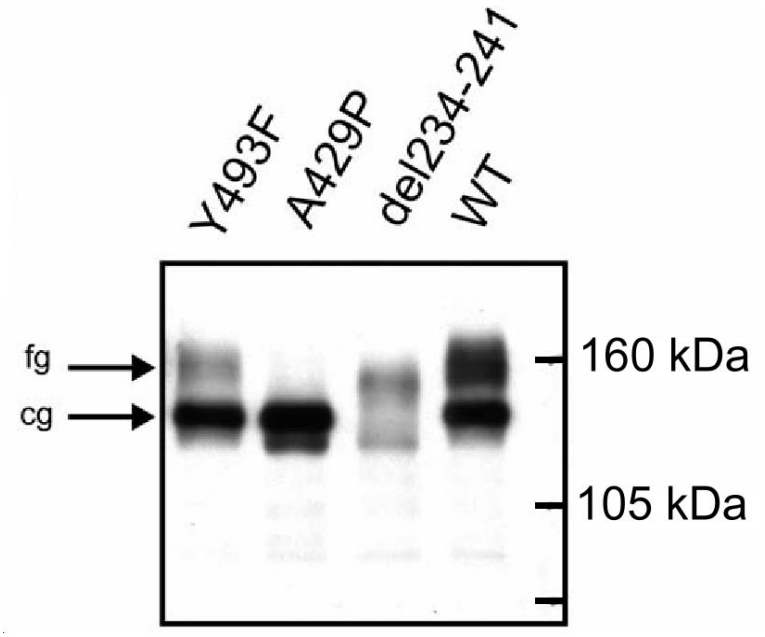


Figure 6

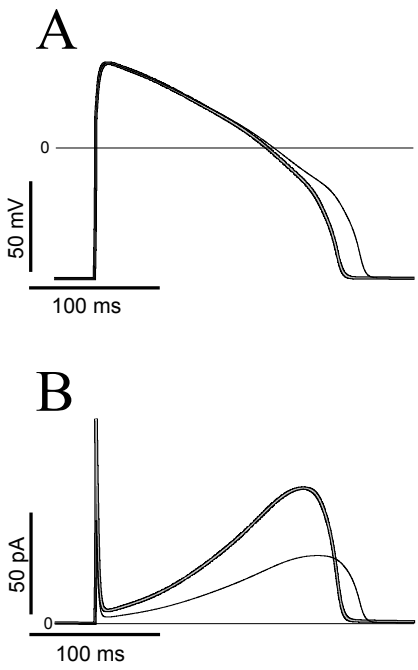


Figure 7